The Astrophysical Journal, 662:544–551, 2007 June 10

THE NEW CLASS OF DUSTY DAZ WHITE DWARFS

Ted von Hippel,[1,2] Marc J. Kuchner,[3] Mukremin Kilic,[4] Fergal Mullally,[1] and William T. Reach[5]
Received 2006 October 9; accepted 2007 March 12

ABSTRACT

Our mid-infrared survey of 124 white dwarfs with the *Spitzer Space Telescope* and the IRAC imager has revealed an infrared excess associated with the white dwarf WD 2115−560 naturally explained by circumstellar dust. This object is the fourth white dwarf observed to have circumstellar dust. All four are DAZ white dwarfs, i.e., they have both photospheric Balmer lines and photospheric metal lines. We discuss these four objects as a class, which we abbreviate "DAZd," where the "d" stands for "dust." Using an optically thick, geometrically thin disk model analogous to Saturn's rings, we find that the inner disk edges are at $\gtrsim$0.1–0.2 $R_\odot$ and that the outer disk edges are $\sim$0.3–0.6 $R_\odot$. This model naturally explains the accretion rates and lifetimes of the detected WD disks and the accretion rates inferred from photospheric metal abundances.

Subject headings: accretion, accretion disks — circumstellar matter — white dwarfs

1. INTRODUCTION

The first white dwarf known to have a dusty debris disk or cloud was G29-38, discovered by Zuckerman & Becklin (1987) to have pronounced excesses in the *K*, *L*, and *M* bands relative to the white dwarf's photosphere. Initially, it was unclear whether the IR excess indicated a substellar companion (Zuckerman & Becklin 1987) or particulate debris. Eventually the near-IR to mid-IR (Tokunaga et al. 1990; Chary et al. 1999) spectral energy distribution (SED), time-resolved photometry in the visible and near-IR that constrained the dust geometry (Graham et al. 1990; Patterson et al. 1991), and limits on the presence of companions from pulsation timing studies (Kleinman et al. 1994) and speckle imaging (Kuchner et al. 1998) argued in favor of particulate debris in a disk. Now new *Spitzer* 7–14 μm spectroscopy (Reach et al. 2005a) shows a strong 10 μm emission feature in the G29-38 excess that can only be caused by small silicate dust particles. If G29-38 has any planets, they are currently undetected (Debes et al. 2005).

While we do not have strong evidence regarding the distribution of the dust around G29-38, we do have a few constraints: the near-IR pulsation data suggest a nonspherical dust distribution (Graham et al. 1990; Patterson et al. 1991), and the particles we see in emission radiate at temperatures of 290–890 K (Reach et al. 2005a). Given the luminosity of the white dwarf (2×10^{-3} $L_\odot$), these temperatures place the dust particles at approximately 0.15 to a few solar radii (Zuckerman & Becklin 1987; Jura 2003; Reach et al. 2005a); the outer radius depends on whether we assume that the dust is in an optically thin or thick component.

G29-38 is a relatively normal, H atmosphere (DA) WD currently passing through its instability strip; it has $T_{\rm eff} \approx 11,800$ K (Kepler & Nelan 1993; Bergeron et al. 1995), $\log g$ from 7.9 (Koester & Wilken 2006) to 8.14 (Bergeron et al. 1995), and an implied mass of 0.56–0.69 $M_\odot$. It has been cooling as a WD for $\sim$0.5 Gyr. The initial-final mass relation of Weidemann (2000) suggests that this range of WD masses corresponds to a zero-age main-sequence (ZAMS) mass of 1.2–3.1 $M_\odot$. G29-38 was therefore once an F or A star (Drilling & Landolt 2000, Table 15.8). G29-38 has photospheric absorption lines from heavy elements (Ca, Mg, Fe; Koester et al. 1997), which makes it a spectral type DAZ. In addition, the photospheric Ca II K line varies in strength on timescales as short as 15 days (von Hippel & Thompson 2007), indicating episodic accretion.

Becklin et al. (2005) and Kilic et al. (2005) recently discovered a second white dwarf with circumstellar dust debris. This object, GD 362, was found to have a broadband, *JHKL′M′* SED that could be fitted by a debris disk (Becklin et al. 2005). Its near-IR spectroscopy shows a strong *K*-band excess without any of the near-IR spectral features of a brown dwarf (Kilic et al. 2005). GD 362 is an H-rich[6] atmosphere WD with metals observed in its photosphere; it is in fact the most metal-rich WD known. It is slightly cooler than G29-38 ($T_{\rm eff} = 9740$ K; Gianninas et al. 2004) yet is substantially more massive at 1.24 $M_\odot$ (Gianninas et al. 2004), which placed it at >7 $M_\odot$ on the main sequence (Weidemann 2000).

A third WD with circumstellar dust, GD 56, was just reported by Kilic et al. (2006a). This star was discovered via its pronounced excess at wavelengths longer than 1.6 μm in low-resolution near-IR spectroscopy. GD 56 is also a DAZ and has $T_{\rm eff} = 14,400$ K and $\log g = 7.8$ (Koester et al. 2005). These reported atmospheric parameters correspond to a low-mass WD (0.52 $M_\odot$), which is expected only for a halo star or a remnant from binary star common envelope evolution. On the other hand, if we assume a slightly higher surface gravity, the inferred mass becomes normal for a Galactic disk WD, e.g., for $\log g = 7.9$, mass = 0.566 $M_\odot$ (Bergeron et al. 1995).

In this paper we report the fourth DAZ with circumstellar dust, WD 2115−560. This WD has $T_{\rm eff} = 9700$ K and $\log g = 8.1$ (Koester et al. 2005), corresponding to a mass of 0.66 $M_\odot$. We discovered this object in our *Spitzer* IRAC 4.5 and 8 μm survey of 124 WDs (Mullally et al. 2007). We conducted this survey to improve on the ground-based *K*-band survey of Zuckerman & Becklin (1992) and Farihi et al. (2005) and the 6.75 μm space-based, ISOCAM survey of Chary et al. (1999) of 11 WDs, none

[1] Department of Astronomy, University of Texas, Austin, TX 78712-0259; ted@astro.as.utexas.edu.
[2] Visiting Scientist, Southwest Research Institute, Boulder, CO 80302.
[3] NASA Goddard Space Flight Center, Greenbelt, MD 20771.
[4] Columbus Fellow, Department of Astronomy, Ohio State University, Columbus, OH 43210.
[5] *Spitzer* Science Center, California Institute of Technology, Pasadena, CA 91125.

[6] D. Koester (2006, private communication) reports that GD 362 has a mixed He/H atmosphere and that the prior mass estimate is substantially too high. This will affect the timescale of gravitational settling and thus the implied accretion rate, but not our analysis.

of which found any new WDs with circumstellar dust. Our survey also aimed to study the photospheres of cool WDs (see Kilic et al. 2006b), which are of great importance to WD cosmochronology, as well as to searches for giant planets and brown dwarfs (see Mullally et al. 2007).

Our discovery of the fourth WD with circumstellar dust leads us to suggest a new class of white dwarfs, the "DAZd" white dwarfs, where "d" indicates circumstellar dust. We choose a lowercase "d" to avoid confusion with double white dwarfs, known as double degenerates and abbreviated "DD." The classification notation for WDs is based on spectroscopic features, and up to now all have been notated by capital letters. Yet these features are all thought to be photospheric, whereas the dust causing the IR excess is circumstellar; a lowercase "d" emphasizes the difference between photospheric and circumstellar spectroscopic properties.

Using the photometry and discovery statistics from our survey, the detailed properties of G29-38 reported by Reach et al. (2005a), and some simple models, we explore the nature and cause of particulate debris in DAZd WDs as a group.

2. OBSERVATIONS

2.1. *Spitzer Data*

Our *Spitzer* survey initially targeted all WDs in the McCook & Sion (1999)[7] catalog brighter than $K_S = 15$ as measured by the Two Micron All Sky Survey (2MASS; Skrutskie et al. 2006), rejecting known binaries and planetary nebulae, yielding a total of 134 WDs. All of these WDs have well-determined positions and most have well-determined proper motions, facilitating (but not guaranteeing complete) cross-referencing between catalogs. We removed one object to avoid a conflict with the *Spitzer* Reserved Observations Catalog, and the time allocation committee removed three other WDs in common with a program focused on DAZ WDs. Our observations for six of these WDs failed to provide quality photometry, mostly because of blending problems, and in the end, we obtained good data for a sample of 124 WDs with $T_{\rm eff} = 5000-60,000$ K, cooling ages from 1 Myr to 7 Gyr, and representing most WD spectral types.

Our observations consisted of five dithers of 30 s each (150 s total integration time) for every WD in our survey. We used the products of the *Spitzer* Science Center pipeline, the basic calibrated data (BCD) frames and the post-BCD frames (mosaics), for our analysis. We used IRAF[8] PHOT and a custom IDL package to perform aperture photometry on individual BCD frames. We also attempted PSF fitting photometry but found that the poorly defined point response function for the IRAC instrument with its large pixels (1.213″ and 1.220″ at 4.5 and 8 μm, respectively) meant that we obtained better results with the IDL and IRAF aperture photometry than with PSF fitting photometry. Both the IDL and IRAF approaches gave identical results, within the errors. In order to maximize the signal-to-noise ratio, we used 5 pixel apertures for bright, isolated objects and 2 or 3 pixel apertures for faint objects or objects in crowded fields. We corrected the resultant fluxes by the aperture correction factors determined by the IRAC team (see the IRAC Data Handbook). For each object, we compared the photometry from 2, 3, and 5 pixel apertures; we found them all to be consistent within the errors.

Following the standard IRAC calibration procedure, we made corrections for the observed array location of each WD before averaging the fluxes of the five frames in each IRAC band. We also performed photometry on the mosaic images and found the results to be consistent with the photometry from individual frames. Based on the calibrations of Reach et al. (2005b), we expect that our IRAC photometry is calibrated to an accuracy of 3%. We estimated the photometric error from the observed scatter in the five images (corresponding to five dither positions) plus the 3% absolute calibration error, added in quadrature. See Mullally et al. (2007) for further details of our reduction procedure.

2.2. *Survey Summary*

Our flux-limited survey of 124 single WDs detected circumstellar dust around two WDs, WD 2115−560 and G29-38, which met the criteria for inclusion in our sample. These two detections among the general population of white dwarfs indicate a detection rate of 1.6% in our flux-limited WD sample. However, other surveys have shown higher circumstellar dust detection rates with more limited samples. Kilic et al. (2006a) found the third circumstellar dust WD candidate, GD 56, in a small survey of DAZ WDs; they estimated that ∼9% of all DAZs have circumstellar dust detectable at *K*. These two samples differ in both wavelength coverage and target selection. The *Spitzer* survey was more sensitive to cooler circumstellar dust. The Infrared Telescope Facility (IRTF) survey of Kilic et al. (2006a) selected WD targets with high atmospheric metal content, the DAZs. The greater sensitivity to WDs with circumstellar dust in the *Spitzer* survey did not yield more such systems; the DAZ survey at the IRTF had a ∼5.6 times higher yield. This result, along with the fact that our new circumstellar dust system, WD 2115−560, turned out to be a DAZ (a fact we did not know when we assembled the sample), suggests a deep connection between detectable circumstellar dust around WDs and the DAZ phenomenon.

Table 1 summarizes the properties of WD 2115−560, along with the three other WDs hosting circumstellar dust already presented in the literature. These WDs span a modest temperature range of 9700–14,400 K, although their mass range is wide for WDs, running from ∼0.56 to ∼1.24 $M_\odot$. This mass and $T_{\rm eff}$ range means that their cooling ages range from ∼0.2 to ≥2.5 Gyr. All four display photospheric metal lines. We list the temperature range of their circumstellar dust from a simple model fit, which we discuss below.

Rounding out the known properties of these WDs, Becklin et al. (2005) and Reach et al. (2005a) find that the fractional luminosity over all wavelengths in the dust is ∼3% in GD 362 and G29-38. The minimum dust mass around G29-38, assuming an optically thin cloud of dust that radiates efficiently in the thermal infrared, is 10^{18} g, approximately equivalent to the mass of a 10 km asteroid.

2.3. *Blackbody Models for the Spectral Energy Distributions*

Perhaps G29-38, the first known and best-studied DAZd, is a good template for understanding this emerging class. Using archival *IUE* spectra, optical photometry from the literature, and *Spitzer* IRAC, IRS, and MIPS data, Reach et al. (2005a) fitted an optically thin dust cloud model to the G29-38 SED. Reach et al. (2005a) showed that a simple model consisting of two modified blackbodies, with temperatures of 290 and 890 K, provided a good fit to the infrared excess.

Their *Spitzer* spectra revealed a strong 10 μm emission feature, well fitted by a combination of forsterite, Mg_2SiO_4, and olivine, $(Mg, Fe)_2SiO_4$. The assumptions of an optically thin dust cloud and blackbody dust place the detectable dust at 1–5 $R_\odot$ from the WD. The Poynting-Robertson (P-R) timescale for particles to spiral onto the WD from a debris reservoir at 1 $R_\odot$ is only 4*a* yr, where *a* is the particle radius in microns. The silicate emission

[7] Also available via the Vizier Online Data Catalog III/235A.

[8] IRAF is distributed by the National Optical Astronomy Observatory, which is operated by the Association of Universities for Research in Astronomy (AURA), Inc., under cooperative agreement with the National Science Foundation.

TABLE 1
White Dwarf and Disk Parameters

Star (1)	Spectral Type (2)	$T_{\rm eff}$ (K) (3)	Mass ($M_\odot$) (4)	ZAMS ($M_\odot$) (5)	WD Age (Gyr) (6)	$L_{\rm dust}$ (%) (7)	Distance (pc) (8)	$T_{\rm dust}$ (K) (9)	$R_{\rm dust}$ ($R_\odot$) (10)	i (deg) (11)	$R_{\rm sub,BB}$ ($R_\odot$) (12)
GD 56	DAZd	14400	0.52–0.57	0.9–1.4	0.2–0.4	4.2	67	1125–525	0.21–0.58	45	0.36
G29-38	DAZd	11600	0.56–0.69	1.2–3.1	0.5	3.5	14	1150–725	0.15–0.28	45	0.18
GD 362	DAZd	9740	1.24	>7.0	>2.5	6.1	24	800–200	0.08–0.50	60	0.07
WD 2115−560	DAZd	9700	0.66	2.8	0.9	0.9	22	900–550	0.17–0.32	80	0.16

Notes.—The sublimation radii (see eq. [2]) assume $T_{\rm sub} = 2000$ K. Mass and cooling ages derived here use the quoted atmospheric parameters and Bergeron et al. (1995) tabulated models. The percentage of luminosity in the disk is the value from our model fits. For G29-38 and GD 362, Reach et al. (2005a) and Becklin et al. (2005) estimate 3% for the disk components of these two WDs, respectively. Distances are from Farihi et al. (2005), van Altena et al. (1995), Gianninas et al. (2004), and Gliese & Jahreiss (1991), respectively. Please see text for references to the atmospheric parameters.

feature observed by Reach et al. (2005a) can only be as strong as it is relative to the continuum (contrast = 125%), if it is emitted by submicron particles. The P-R timescale for such tiny particles is years or less.

Radiation pressure can eject small grains in orbit around a star (e.g., Wyatt & Whipple 1950). A spherical blackbody grain with radius $r_{\rm grain}$ and density $\rho_{\rm grain}$ (in g cm^{-3}) will be ejected from bound orbit around a WD by radiation pressure if $r_{\rm grain} < r_{\rm blowout}$, where

$$r_{\rm blowout} = (1.15\ \mu{\rm m})\rho_{\rm grain}\frac{L_{\rm WD}}{L_\odot}\frac{M_\odot}{M_{\rm WD}}. \quad (1)$$

However, for a typical WD luminosity, $L_{\rm WD} = 10^{-3}\ L_\odot$, and WD mass, $M_{\rm WD} = 0.6\ M_\odot$, the blowout size given by this standard equation is 0.002 μm, much smaller than the peak wavelength of the stellar blackbody emission, suggesting that even these small grains may survive around the WD.

2.4. *Flat-Disk Models for the Spectral Energy Distributions*

An optically thin dust cloud would have a lifetime no longer than the short P-R timescale. Therefore, it seems likely that the dust cloud is optically thick, shielding much of the dust from the stellar radiation that causes P-R drag. With this idea in mind, we fit the SEDs of each of the four WD debris systems using standard optically thick flat-disk models (Friedjung 1985; Jura 2003). We derived the input spectra for these simple disk models by fitting blackbody curves to the photospheric portions of the SEDs and then used the models to derive disk inclinations and dust temperatures that correspond to the inner and outer radii of the disks.

For each WD, we created a grid of models with inner disk temperatures $T_{\rm in} = 600$–1250 K, outer disk temperatures $T_{\rm out} = 200$–1175 K, $T_{\rm in} > T_{\rm out}$, and a range of inclination angles. We then found the model that best fitted the IR photometry of each WD (J band and beyond) by minimizing χ^2. Table 1 lists the temperature ranges and inclinations of the best-fit models.

For GD 56 and GD 362 we included the IRTF spectroscopy of Kilic et al. (2005, 2006a) in the data to be fitted. For G29-38 we performed one fit using our *Spitzer* photometry and another fit using the IRTF (Tokunaga et al. 1990) plus *Infrared Space Observatory* (*ISO*) photometry (Chary et al. 1999), although without the 10.5 μm photometry, which is likely to be influenced by the strong silicate emission feature. The fit to the older IRTF and *ISO* photometry was poorer than the fit to the *Spitzer* data, and we report only the fit to the modern data in Table 1. The difference between the *Spitzer* and older data sets most likely reflects calibration errors that plagued the ground-based and particularly the *ISO* photometry (R. Chary & B. Zuckerman 2006, private communication). It is also possible that the G29-38 debris disk has evolved substantially over the 15 yr span of these observations.

Figures 1–4 present our best-fit debris disk models. All four DAZd WDs show a pronounced IR excess relative to the expected WD photospheres, represented by the WD model atmospheres (*solid lines*; kindly provided by Detlev Koester). The debris disk components (*dashed lines*) fit the near-IR and mid-IR excess well.

Table 1 also lists the inner and outer radii of the best-fit flat-disk models. They range from 0.15 to 0.58 $R_\odot$, or 13 to 49 white dwarf radii, for the three normal mass WDs and from 0.08 to 0.50 $R_\odot$, or 17 to 106 white dwarf radii, for GD 362, assuming the high-mass value currently in the literature, which implies a much smaller radius. The disk model has no explicit inner edge directly exposed to radiation from the WD, and thus the inner radii are significantly underestimated.

3. A POSSIBLE PHYSICAL DESCRIPTION OF THE DISKS

Perhaps the observations of DAZ disks all point to a common simple picture originally suggested by Jura (2003); the disks are analogs of planetary rings, physically thin disks of rocks and dust with optical depth ≈1. Our new data make this analogy much more compelling. As shown above, the physically thin, optically thick disk geometry implied by this picture can match the observed SEDs of DAZd WDs. Besides providing an excuse for

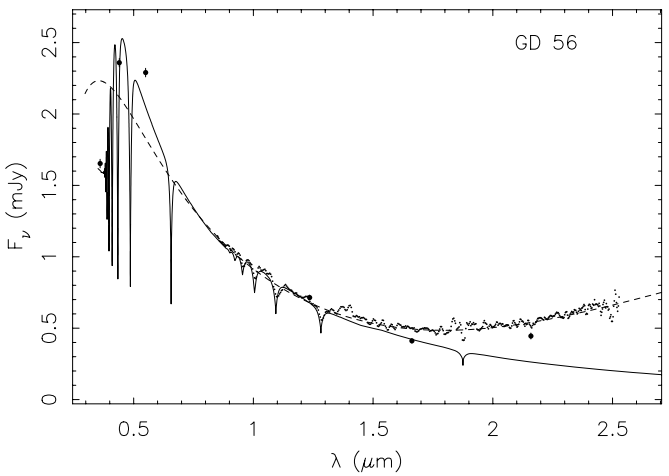

Fig. 1.—Debris disk model and observations for GD 56. Closely spaced black dots represent the 0.8–2.5 μm spectrum obtained at the IRTF (Kilic et al. 2006a). The larger black dots with error bars typically smaller than the symbol size represent the *UBV* photometry from McCook & Sion (1999) and the *JHK* photometry from 2MASS (Skrutskie et al. 2006). The dashed line represents our fitted debris disk model, with $T_{\rm in} = 1125$ K and $T_{\rm out} = 525$ K. For comparison purposes, the solid line represents a WD model atmosphere with $T_{\rm eff} = 14{,}000$ K and $\log g = 8.0$, kindly provided by Detlev Koester.

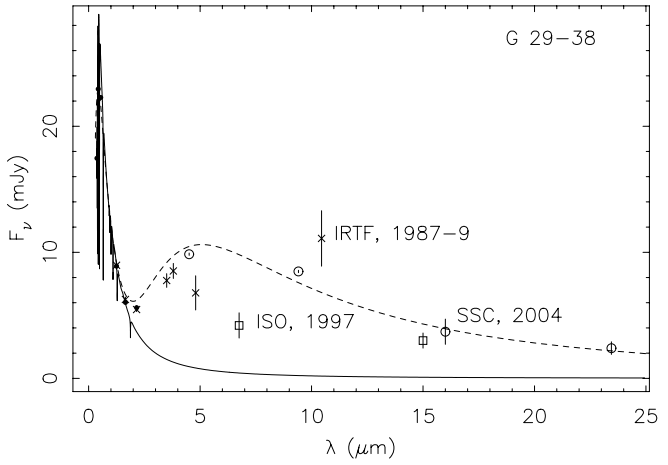

FIG. 2.—Similar to Fig. 1, but for G29-38. More extensive IR photometry is available for this object. Crosses represent the IRTF photometry of Tokunaga et al. (1990; data obtained during 1987–1989). Squares represent the *ISO* photometry obtained by Chary et al. (1999; observed 1997 December 11). Our *Spitzer* data are represented by the open circles. The error bars in the IRAC bands are smaller than the symbol size. We do not plot the near-IR spectra from IRTF to avoid crowding in this figure. Our debris disk model for G29-38 has $T_{\rm in} = 1150$ K and $T_{\rm out} = 725$ K.

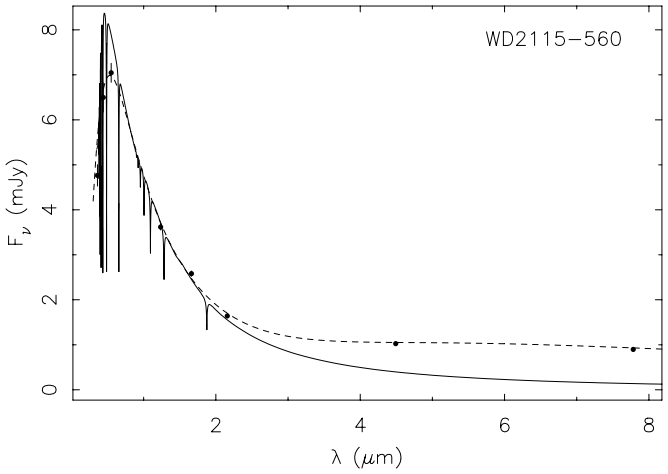

FIG. 4.—Similar to Fig. 1, but for WD 2115−560. Optical photometry from McCook & Sion (1999), near-IR photometry from 2MASS (Skrutskie et al. 2006), and our IRAC photometry for WD 2115−560 fit a debris disk model with $T_{\rm in} = 900$ K and $T_{\rm out} = 550$ K. The lower overall disk flux is best fitted by a nearly edge-on disk; $i \approx 80^\circ$.

that disk geometry, the planetary ring analogy has the following virtues:

1. This picture naturally incorporates both small dust grains and larger, long-lived source particles. Standard models of planetary rings (e.g., Cuzzi et al. 1979) contain a distribution of particle sizes. The largest ring particles contain most of a ring's mass. These particles occupy a "monolayer" a few particle widths thick, while the smaller particles, like the ones observed to produce the 10 μm emission feature in G29-38 (Reach et al. 2005a), are spread over a thicker polylayer. Planetary rings may also consist of dusty rings interspersed with rings of larger bodies (e.g., de Pater et al. 2006). The small particles are continually produced by the collisions of the larger particles and protected to some degree from radiation forces by the optical thickness of the ring.

2. This picture provides a disk lifetime consistent with the ages of the DAZd WDs. An optically thick disk of rocks has a lifetime set by the viscous spreading time of the ring, $t_{\rm visc} \approx r^2/\nu$, where r is the radius of the ring and ν is the kinematic viscosity. To estimate the disk lifetime, let us assume that the viscosity of the WD rings is similar to that of Saturn's rings. The viscosity of a monolayer ring is $\nu = \Omega\tau R_\nu$, where τ is the optical depth and R_ν is a representative particle size, weighted toward the larger particles (Goldreich & Tremaine 1982). The angular speed in the WD ring is similar to that in planetary rings: $\Omega \approx 2 \times 10^{-4}$ s^{-1}. So assuming a similar viscosity for the WD debris disks and Saturn's rings is like assuming a similar optical depth and particle size distribution. With this assumption, the WD ring lifetimes are $\sim$100 times longer than the lifetime of Saturn's rings because of their larger radii. This lifetime is easily $\gtrsim 10^9$ yr, comparable to the median post–main-sequence lifetime of the WDs in our survey. In this picture, WD rings do not require continual replenishment from a longer lived source of small bodies.

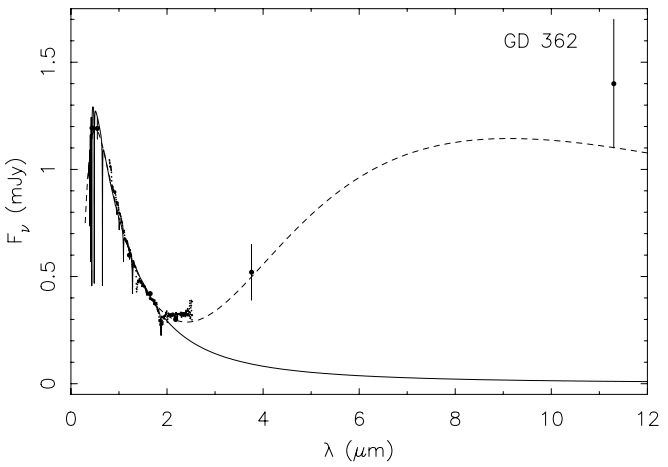

FIG. 3.—Similar to Fig. 1, but for GD 362. The L' and N' photometry was obtained at Gemini (Becklin et al. 2005). We do not use the N' photometry in deriving the debris disk parameters since it was likely influenced by the silicate emission band. Our debris disk model for GD 362 has $T_{\rm in} = 800$ K and $T_{\rm out} = 200$ K.

3. This picture implies a metal accretion rate consistent with the photospheric abundances of metals in the DAZd WDs. In the context of this picture, we can estimate the mass of a typical DAZd disk as $\pi r_{\rm out}^2 \Sigma$, using the surface density of Saturn's rings ($\Sigma \approx 40$ g cm^{-2}; Tiscareno et al. 2007) and an outer radius $r_{\rm out} \approx 1.5\ R_\odot$ (see item 5, below). With these assumptions, we find a representative disk mass of $\sim 2 \times 10^{-4}\ M_\oplus$. If the accretion time is 10^9 yr, the resulting accretion rate onto the WD is $\sim 7 \times 10^{-19}\ M_\odot$ yr^{-1}.

Figure 5 shows the observed photospheric abundances derived by Koester & Wilken (2006) for a large sample of DAZ WDs. Figure 6 shows accretion rates for this sample inferred from these photospheric abundances and the atmospheric residence times Koester & Wilken (2006) derived for these WDs. These accretion rates from Koester & Wilken (2006) are based on an assumption that the accreted material has solar composition. Our model assumes that the material is mostly refractory, so to compare our accretion rate to Figure 6, we need to multiply it by a factor of 50, giving us $\sim 3 \times 10^{-17}\ M_\odot$ yr^{-1}. This accretion rate sits right in the middle of the range of DAZ inferred accretion rates and is only about an order of magnitude less than that of the known DAZd's. It is easy to imagine a disk with slightly higher surface density or viscosity than Saturn's rings that would precisely match the DAZd accretion rates in Figure 6.

4. This picture explains the inner radii of DAZd disks inferred from their SEDs. The radius where the equilibrium temperature of a dust grain exceeds the sublimation temperature, $T_{\rm sub}$, for the grains should mark the inner boundary of the ring. Although

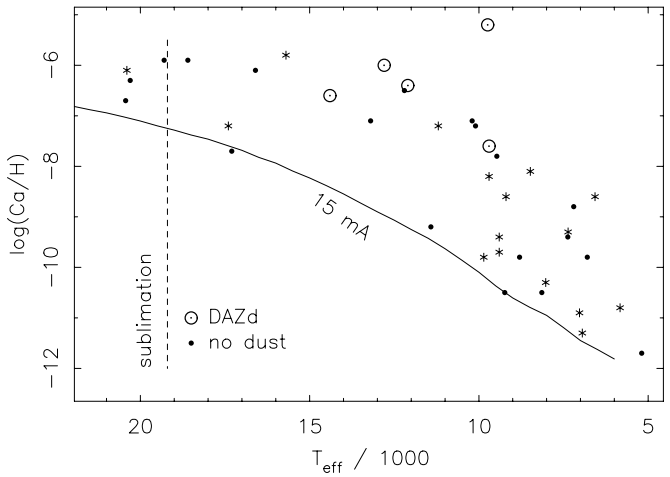

FIG. 5.—$T_{\rm eff}$ vs. log (Ca/H) for DAZs from the sample of Koester & Wilken (2006). The solid diagonal line is the approximate lower limit calcium abundance for discovery from Koester & Wilken (2006), at an equivalent width of 15 mÅ. The dashed vertical line is the approximate dividing stellar $T_{\rm eff}$ at which blackbody dust inside the tidal destruction radius of the WD will be completely sublimated for $T_{\rm sub} = 1200$ K. Other sublimation temperatures and dust properties move this dividing line a few thousand degrees (see text). The open symbols with dots in their centers are the known DAZd WDs. Besides the four DAZd WDs discussed here, we also plot an additional DAZd just found by Kilic & Redfield (2007) via IRTF spectroscopy. The filled circles are DAZs with no detected dust excesses in either the IRTF study of Kilic et al. (2006a) or our *Spitzer* observations. The remainder (plotted with asterisks) of the DAZs have not yet been searched for debris disks.

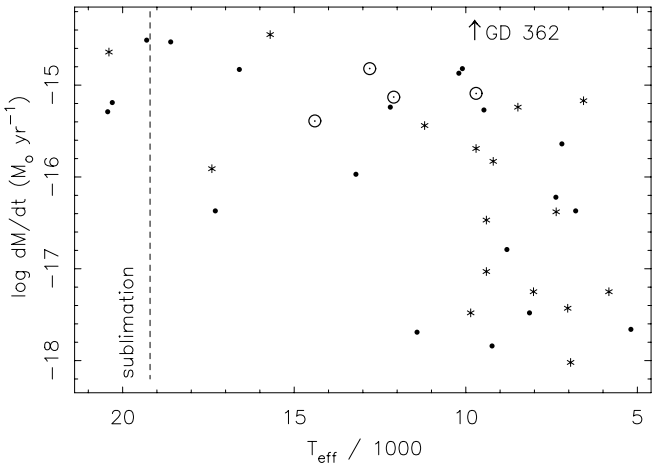

FIG. 6.—$T_{\rm eff}$ vs. the log of the accretion rate in solar masses per year, assuming the accretion of solar abundance material, from Koester & Wilken (2006). The symbols are the same as in Fig. 5, although GD 362, with log $(dM/dt) \approx -12.09$, is not plotted for clarity.

most of the disk sees only stellar radiation at an oblique angle, the inner radius of the disk can see direct stellar radiation, so it should be hotter than the flat-disk model would predict, closer to the temperature of an optically thin dust cloud, or a single grain in free space. With this geometry in mind, we find that for blackbody grains, the sublimation radius is

$$R_{\rm sub,\,BB} = \frac{1}{2}\left(\frac{T_{\rm sub}}{T_\odot}\right)^{-2}\left(\frac{L_{\rm WD}}{L_\odot}\right)^{1/2} R_\odot, \qquad (2)$$

where $L_{\rm WD}$ is the WD luminosity. For a typical WD luminosity, $L_{\rm WD} = 10^{-3}\ L_\odot$, and assuming a silicate sublimation temperature, $T_{\rm sub} = 1500$ K, equation (2) gives $R_{\rm sub} = 0.24\ R_\odot$.

Another component of the disks may be grains too small to efficiently emit at the blackbody peak wavelength. These grains are slightly hotter than blackbody grains at the same location in the nebula, so they sublimate at larger radii. For example, for the "medium"-sized grains described by Backman & Paresce (1993), the sublimation radius is

$$R_{{\rm sub},M} = \left(\frac{T_{\rm sub}}{4009.21}\right)^{-5/2}\left(\frac{L_{\rm WD}}{L_\odot}\right)^{1/2} \lambda_0^{-1/2}\ R_\odot, \qquad (3)$$

where λ_0 is the grain size measured in microns. For the same assumed WD luminosity and silicate sublimation temperature, and for a grain size of 1 μm, $R_{{\rm sub},M} = 0.37\ R_\odot$.

Column (12) of Table 1 lists dust sublimation radii for each of the DAZd's calculated from equation (2) assuming $T_{\rm sub} = 2000$ K. This assumption produces a good match to the inner radii inferred from our models of the SEDs. However, we did not incorporate the physics of direct heating of the inner rim of the disk into our SED modeling, so we cannot compare sublimation radii calculated using the assumption of direct heating to the radii inferred from our flat-disk models. We can, however, compare the inner temperatures inferred from our flat-disk models to the sublimation temperatures of typical dust materials and retain self-consistency. Column (9) of Table 1 lists the temperatures of the inner and outer edges of the disks inferred from the flat-disk models. The temperatures at the inner edge range from 800 to 1150 K.

5. This picture explains the outer radii of DAZd disks inferred from their SEDs. A dynamically cold ring cannot extend much beyond the Roche radius; beyond this radius, the ring particles coagulate into moons or, in the case of the white dwarf rings, asteroids or planets. The Roche radius for tidal disruption of an asteroid near a WD is given by Jura (2003):

$$R_{\rm Roche} = C_{\rm tide}\, R_{\rm WD}\left(\frac{\rho_{\rm WD}}{\rho_{\rm asteroid}}\right)^{1/3}, \qquad (4)$$

where $C_{\rm tide}$ is a parameter of order unity that depends on the asteroid's composition, orbit, and rotation, $R_{\rm WD}$ is the radius of the WD, $\rho_{\rm WD}$ is the density of the WD, and $\rho_{\rm asteroid}$ is the density of the asteroid. For G29-38, $R_{\rm Roche} \approx 126 C_{\rm tide}\, R_{\rm WD} \approx 1.5 C_{\rm tide}\, R_\odot \approx 1.5\ R_\odot$. Since this equation only includes density to the one-third power and WD masses span a narrow range ($\sim$0.55–1.2 $M_\odot$), all WDs have about the same Roche radii.

Jura (2003) pointed out that the outer radius of the disk around G29-38 roughly matched the Roche radius for this WD. We find that the outer radii of all the DAZd disks as inferred from physically thin, optically thick disk models for the SEDs are consistent with the WD Roche radii.

6. This picture may explain the absence of dust around luminous DAZ white dwarfs. This *Spitzer* survey and the survey of Kilic et al. (2006a) examined 11 DAZ white dwarfs hotter than 15,000 K and found circumstellar dust around none of them (see Figs. 5 and 6). The high surface abundances and very short atmospheric residence times for calcium (see § 4) in these 11 stars made them excellent candidates to host observable debris disks. Gänsicke et al. (2006) discovered a single WD with effective temperature $\sim$22,000 K that hosts a calcium gas disk but shows no sign of circumstellar dust. These observations suggest that perhaps hotter, more luminous WDs cannot host dust.

The analogy between WD disks and planetary rings suggests a natural interpretation of these observations; for hot WDs, the sublimation zone reaches beyond the Roche radius. These WDs, like main-sequence stars, lack a circumstellar region where small bodies

are stable against both sublimation and coagulation in dynamically cold disks.

We can find the critical WD effective temperature above which this stable region disappears by setting $R_{\rm sub,\,BB} = R_{\rm Roche}$, assuming blackbody dust grains:

$$T_{\rm crit,\,BB} = \sqrt{2C_{\rm tide}}\left(\frac{\rho_{\rm WD}}{\rho_{\rm asteroid}}\right)^{1/6} T_{\rm sub}. \quad (5)$$

Ignoring the slow dependence of this expression on the WD density, we find that the critical WD temperature is $T_{\rm crit,\,BB} \approx 16T_{\rm sub}$. If instead we use the 1 μm "medium" grains of Backman & Paresce (1993), we find that the maximum WD temperature for hosting a dust disk is

$$T_{{\rm crit},M} = 0.13\sqrt{C_{\rm tide}}\left(\frac{\rho_{\rm WD}}{\rho_{\rm asteroid}}\right)^{1/6} T_{\rm sub}^{5/4}, \quad (6)$$

so $T_{\rm crit,\,M} \approx 1.5T_{\rm sub}^{5/4}$.

For grains with $T_{\rm sub} = 1500$ K, we find $T_{\rm crit,\,BB} = 24,000$ K and $T_{{\rm crit},M} = 14,000$ K. We suggested above that the inner edges of the observed DAZd disks match blackbody grains with $T_{\rm sub} = 2000$ K. This combination implies that there should be no disks around WDs hotter than $T_{\rm crit,\,BB} = 32,000$ K, keeping in mind the caveats described above. The observations described above suggest that the critical temperature should be roughly 15,000–22,000 K. These observations broadly agree with the hypothesis that the grain sublimation temperature and the Roche radius together limit the kinds of WDs that can host dust disks, although clearly details remain to be better understood.

4. THE CONNECTION BETWEEN WD DEBRIS SYSTEMS AND THE DAZ PHENOMENON

As we mentioned above, the presence of photospheric metals in DAZs implies ongoing accretion of these metals. Our physical model for the DAZd disks provides a natural explanation for this accretion. Let us examine in more detail the connection between DAZd disks and the DAZ phenomenon.

White dwarfs are classified as DAZ or DBZ if their optical spectra contain metal lines along with much stronger hydrogen or helium lines, respectively. White dwarfs showing metal lines may also be classified simply DZ if they are too cool to show hydrogen or helium lines. Hybrid types, such as DABZ, also exist.

Since the discovery of metal lines in WD atmospheres (see Weidemann 1958; Greenstein 1960, p. 692), the origin of these metals has been debated (e.g., Lacombe et al. 1983; Aannestad et al. 1993; Dupuis et al. 1993; Zuckerman & Reid 1998; Zuckerman et al. 2003; Koester & Wilken 2006; Kilic & Redfield 2007). The high surface gravity of WDs should cause the denser atoms of the metals to sink in the atmosphere on timescales of days to millions of years, depending on the atmospheric constituents, effective temperature, and WD mass. These timescales are all much shorter than the ages of most WDs.

Figure 7 shows the timescale for gravitational settling for DA WDs with $\log g = 7.75$–9.0 and mass of roughly 0.48–1.20 $M_\odot$, taken from Koester & Wilken (2006). For comparison, the four DAZd stars are plotted on this figure based on their atmospheric $T_{\rm eff}$ and $\log g$ values. Figure 7 shows that for the WDs hotter than 11,000 K, the settling times are substantially less than a year, and even for our coolest, low surface gravity object, WD 2115−560, the settling time is still less than 200 yr.

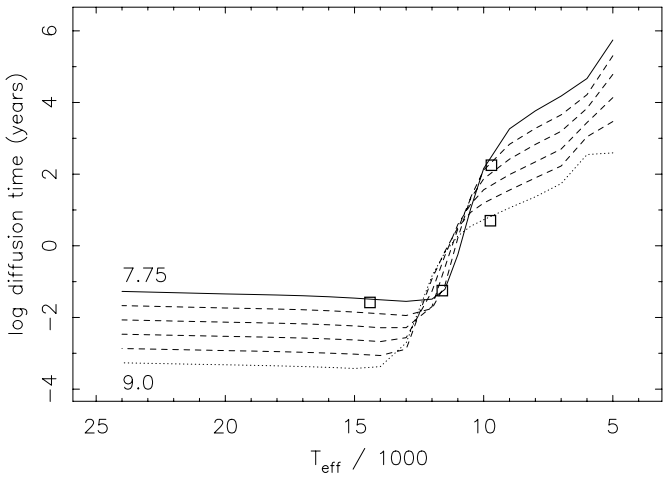

FIG. 7.—Timescale for gravitational settling of calcium (Koester & Wilken 2006). The locations of the four DAZd WDs are indicated by the open squares. All have short settling times.

These short settling timescales imply that DAZ stars were very recently accreting heavy elements. Interstellar accretion, perhaps the most discussed scenario for supplying the heavy elements, seems to fail by orders of magnitude for many of the known DAZ WDs (Aannestad et al. 1993; although see the counterargument by Koester & Wilken 2006). However, such accretion would be natural if DAZ WDs typically harbor substantial circumstellar disks.

So far all debris WD systems with circumstellar disks have detectable photospheric metal lines. Is it possible that all metal-rich WDs (DAZ/DBZ/DZ) accrete their metals via debris disks?

One reason answering this question is difficult is that not all WDs with photospheric metals can be recognized as DAZ/DBZ/DZs. This point is made in Figure 5, where the solid line indicating a constant Ca equivalent width of 15 mÅ corresponds to much higher Ca abundances for hotter WDs than for cooler WDs. It is much more difficult to recognize a DAZ at higher stellar temperatures. Figure 6 shows another view of the same data, easier to grasp visually, but more model dependent. The maximum accretion rates necessary to explain the observed abundances are essentially independent of $T_{\rm eff}$; the short atmospheric residence timescales for the hot WDs are balanced by the deeper convective reservoirs for the cooler WDs.

The DAZd WDs are located near the top of Figures 5 and 6; they are among the WDs with the highest photospheric heavy-element abundances and the highest inferred accretion rates and therefore should harbor the most massive and easiest to detect of the debris disks. It thus seems possible that the debris disks found to date display an observational selection effect and that the majority of DAZs harbor debris disks.

For all DAZd WDs except the possibly massive GD 362, Koester & Wilken (2006) find accretion rates in the narrow range of $(4.07$–$8.13) \times 10^{-16}\ M_\odot\ {\rm yr}^{-1}$. Koester & Wilken (2006) assumed that the accreted material had solar abundances. We assume instead that the accreted material lacks hydrogen and helium, reducing the total accretion rate by a factor of 50. This lower limit corresponds to $(8$–$16) \times 10^{-18}\ M_\odot\ {\rm yr}^{-1}$ or $(1.6$–$3.2) \times 10^{16}\ {\rm g\ yr}^{-1}$ of refractory elements fed to the WD, a rate consistent with viscous accretion in our planetary ring model. If this accretion persists for at least 25% of the lifetime of the WDs, commensurate with the fraction of DAs that are DAZs (Zuckerman et al. 2003), it corresponds to an accreted mass of $\gtrsim 7 \times 10^{-4}\ M_\oplus$ accreted over 1 Gyr.

4.1. *Origin of the Debris*

We have discussed the basic properties of the debris systems found to date and have connected the debris observable in the infrared to the photospheric metal lines observable in the optical. We have argued that dust debris is common around WDs and that this dust must be steadily accreting onto the WD. We have not yet examined possible sources for the debris around WDs. Here we consider possible origins: WD mergers, debris left during the asymptotic giant branch (AGB) or proto–planetary nebula (pPN) phases, and accretion of dust derived from planetary system bodies.

4.1.1. *White Dwarf Mergers*

Merging WDs are expected to leave behind disks (Livio et al. 2005; Hansen et al. 2006) to shed angular momentum. According to the calculations of Livio et al. (2005), such disks should be massive ($\sim$0.007 $M_{\odot}$), extend to 1 AU or more, and be predominantly composed of carbon and oxygen, assuming the merger of two WDs each with mass $\leq$0.7 $M_{\odot}$. The minimum mass for most of these merged WDs ought to be $\geq$1.1 $M_{\odot}$, since it takes about 10 Gyr to produce a 0.55 $M_{\odot}$ WD.

Except for GD 362, with a mass possibly equal to 1.24 $M_{\odot}$, these mass constraints rule out this explanation for the majority of DAZd WDs. The other WDs with circumstellar dust have masses ranging from 0.52 to 0.69 $M_{\odot}$. In addition, the disk mass and radial extent appear inconsistent with all DAZd stars discovered to date. While WD mergers must be taking place, and they may possibly be the source of the disk around GD 362, they are not the source of the majority of the observed DAZd systems.

4.1.2. *Late Stages of Stellar Evolution*

The outflows of late-stage AGB stars and pPNe are often highly nonspherical. This process is not understood, and a range of models have been proposed for the origin of the asymmetries, including stellar companions and magnetic fields (see Balick & Frank 2002 and references therein). There is circumstantial evidence for the formation of disks and tori during the AGB to post-AGB star transition, albeit at much greater distances from the host star, and most pPNe are producing or have recently produced dust particles (Balick & Frank 2002). In particular, Waters et al. (1998) observed olivines and pyroxenes around a pre–white dwarf. While most of the outflows are ejected well above the stars' escape velocities, at present it is not known whether some small fraction of these outflows remain in orbit after they are ejected. Remaining stellar material is a possible explanation for the dust disk discovered by Su et al. (2007) around (at 35–150 AU) the Helix planetary nebula. While Su et al. (2007) attribute the observed dust to disrupted Kuiper Belt objects or disrupted comets, it could also be the result of stellar material ejected with less than the escape speed.

This scenario predicts dusty environments for the youngest WDs with less and less dust as WDs age. The observations, however, run counter to this. All four of the known DAZd systems have old host WDs with ages from $\geq$0.2 to $\geq$2.5 Gyr, and no hot, dusty WDs have been discovered. The metal disk WD found by Gänsicke et al. (2006) pushes this to slightly younger objects, $\sim$0.1 Gyr, but still, if the late stages of stellar evolution commonly leave debris disks at a range of radii, these debris disks should be detectable in our survey and in *IUE* observations of hot WDs. Yet, to date, no such systems have been seen (Hansen et al. 2006; Kilic et al. 2006a).

4.1.3. *Planetary System Remnants*

The dust around DAZd's may represent the remains of planetary systems. Roughly 5%–10% of A-type stars have substantial debris disks (e.g., Backman & Paresce 1993), and precise Doppler surveys find giant planets around roughly 5%–10% of solar-type stars (e.g., Fischer & Valenti 2005). Perhaps 5%–10% or more of WD progenitors had planetary systems, and some small bodies in these systems survived the post–main-sequence evolution of their host stars (Debes & Siguardsson 2002; Jura 2003). Our observations and models appear to be consistent with this picture for the origin of all the DAZd disks.

5. CONCLUSIONS

We presented the properties of WD 2115−560, a new WD with infrared excess we discovered in our *Spitzer* IRAC photometry, and the fourth DAZ seen to have an infrared excess well described by circumstellar dust debris. We examined the dusty DAZ WDs as a class, which we refer to with the letters "DAZd."

Using a simple, flat, optically thick disk model motivated by the geometry of Saturn's rings, we find that the dust in these four DAZd WDs resides in disks ranging in inner temperature from $\sim$800 to 1150 K and outer temperature from $\sim$200 to 725 K, not taking into account the direct heating of the inner edges of the disks. The outer disk temperatures are likely to be lower limits set by the sensitivity of the observations and the amount of dust radiating at that temperature. These dust temperatures imply that the inner disk edges are at $\gtrsim$0.1–0.2 $R_{\odot}$ and the detectable extent of the outer disks is $\sim$0.3–0.6 $R_{\odot}$. The close circumstellar locations of these debris disks are consistent with simple sublimation calculations and with the Roche radius for tidal disruption of an asteroid near a WD (Jura 2003).

We find that, taken together, the DAZd WDs point to a disk model analogous to planetary rings. This model naturally explains the disk accretion rates and lifetimes and the temperature distribution of the dusty WDs. We favor the interpretation that most of these disks represent planetary system remnants.

This work is based in part on observations made with the *Spitzer Space Telescope*, which is operated by the Jet Propulsion Laboratory, California Institute of Technology under NASA contract 1407. Support for this work was provided by NASA through award project NBR 1269551 issued by JPL/Caltech to the University of Texas.

REFERENCES

Aannestad, P. A., Kenyon, S. J., Hammond, G. L., & Sion, E. M. 1993, AJ, 105, 1033
Backman, D. E., & Paresce, F. 1993, in Protostars and Planets III, ed. E. H. Levy & J. I. Lunine (Tucson: Univ. Arizona Press), 1253
Balick, B., & Frank, A. 2002, ARA&A, 40, 439
Becklin, E. E., Farihi, J., Jura, M., Song, I., Weinberger, A. J., & Zuckerman, B. 2005, ApJ, 632, L119
Bergeron, P., Wesemael, F., & Beauchamp, A. 1995, PASP, 107, 1047
Chary, R., Zuckerman, B., & Becklin, E. E. 1999, in The Universe as Seen by *ISO*, ed. P. Cox & M. F. Kessler (ESA-SP 427; Garching: ESA), 289
Cuzzi, J. N., Burns, J. A., Durisen, R. H., & Hamill, P. M. 1979, Nature, 281, 202
Debes, J., & Siguardsson, S. 2002, ApJ, 572, 556
Debes, J., Siguardsson, S., & Woodgate, B. E. 2005, ApJ, 633, 1168
de Pater, I., Hammel, H. B., Gibbard, S. G., & Showalter, M. R. 2006, Science, 312, 92
Drilling, J. S., & Landolt, A. U. 2000, in Allen's Astrophysical Quantities, ed. A. N. Cox (4th ed.; New York: Springer), 388
Dupuis, J., Fontaine, G., & Wesemael, F. 1993, ApJS, 87, 345
Farihi, J., Becklin, E. E., & Zuckerman, B. 2005, ApJS, 161, 394
Fischer, D. A., & Valenti, J. 2005, ApJ, 622, 1102

Friedjung, M. 1985, A&A, 146, 366
Gänsicke, B. T., Marsh, T. R., Southworth, J., & Rebassa-Mansergas, A. 2006, Science, 314, 1908
Gianninas, A., Dufour, P., & Bergeron, P. 2004, ApJ, 617, L57
Gliese, W., & Jahreiss, H. 1991, The Third Catalog of Nearby Stars (Heidelberg: Astron. Rech. Inst.)
Goldreich, P., & Tremaine, S. 1982, ARA&A, 20, 249
Graham, J. R., Matthews, K., Neugebauer, G., & Soifer, B. T. 1990, ApJ, 357, 216
Greenstein, J. L., ed. 1960, Stellar Atmospheres (Chicago: Univ. Chicago Press)
Hansen, B. M. S., Kulkarni, S., & Wiktorowicz, S. 2006, AJ, 131, 1106
Jura, M. 2003, ApJ, 584, L91
Kepler, S. O., & Nelan, E. P. 1993, AJ, 105, 608
Kilic, M., & Redfield, S. 2007, ApJ, 660, 641
Kilic, M., von Hippel, T., Leggett, S. K., & Winget, D. E. 2005, ApJ, 632, L115
———. 2006a, ApJ, 646, 474
Kilic, M., von Hippel, T., Mullally, F., Reach, W. T., Kuchner, M. J., Winget, D. E., & Burrows, A. 2006b, ApJ, 642, 1051
Kleinman, S. J., et al. 1994, ApJ, 436, 875
Koester, D., Provencal, J., & Shipman, H. L. 1997, A&A, 320, L57
Koester, D., Rollenhagen, K., Napiwotzki, R., Voss, B., Christlieb, N., Homeier, D., & Reimers, D. 2005, A&A, 432, 1025
Koester, D., & Wilken, D. 2006, A&A, 453, 1051
Kuchner, M. J., Koresko, C. D., & Brown, M. E. 1998, ApJ, 508, L81
Lacombe, P., Wesemael, F., Fontaine, G., & Liebert, J. 1983, ApJ, 272, 660
Livio, M., Pringle, J. E., & Wood, K. 2005, ApJ, 632, L37
McCook, G. P., & Sion, E. M. 1999, ApJS, 121, 1
Mullally, F., Kilic, M., Reach, W. T., Kuchner, M. J., von Hippel, T., Burrows, A., & Winget, D. E. 2007, ApJS, in press (astro-ph/0611588)
Patterson, J., Zuckerman, B., Becklin, E. E., Tholen, D. J., & Hawarden, T. 1991, ApJ, 374, 330
Reach, W. T., Kuchner, M. J., von Hippel, T., Burrows, A., Mullally, F., Kilic, M., & Winget, D. E. 2005a, ApJ, 635, L161
Reach, W. T., et al. 2005b, PASP, 117, 978
Skrutskie, M. F., et al. 2006, AJ, 131, 1163
Su, K. Y. L., et al. 2007, ApJ, 657, L41
Tiscareno, M. S., Burns, J. A., Nicholson, P. D., Hedman, M., & Porco, C. C. 2007, Icarus, in press (astro-ph/0610242)
Tokunaga, A. T., Becklin, E. E., & Zuckerman, B. 1990, ApJ, 358, L21
van Altena, W. F., Lee, J. T., & Hoffleit, E. D. 1995, The General Catalogue of Trigonometric Stellar Parallaxes (4th ed.; New Haven: Yale Univ. Obs.)
von Hippel, T., & Thompson, S. E. 2007, ApJ, 661, 477
Waters, L. B. F. M., et al. 1998, Nature, 391, 868
Weidemann, V. 1958, PASP, 70, 466
———. 2000, A&A, 363, 647
Wyatt, S. P., & Whipple, F. L. 1950, ApJ, 111, 134
Zuckerman, B., & Becklin, E. E. 1987, Nature, 330, 138
———. 1992, ApJ, 386, 260
Zuckerman, B., Koester, D., Reid, I. N., & Hünsch, M. 2003, ApJ, 596, 477
Zuckerman, B., & Reid, I. N. 1998, ApJ, 505, L143